

# Surfactant Distribution in Waterborne Acrylic Films. 1. Bulk Investigation

Céline Arnold, Fabrice Thalmann, Carlos Marques, Pascal Marie, and Yves Holl\*

Institut Charles Sadron, CNRS UPR 22, Université de Strasbourg, 23 rue du Loess,  
BP 84047, 67034 Strasbourg Cedex 2, France

Received: April 14, 2010; Revised Manuscript Received: June 11, 2010

The distribution of an anionic surfactant, sodium dodecyl sulfate (SDS), in waterborne acrylic films was investigated, focusing on the effects of particle composition and size, and pH of the latex. The observed surfactant distributions could be classified in two categories: homogeneous and heterogeneous, the latter showing SDS aggregates. The shape of the profiles was related to the stability of the latex during drying, at short interparticular distances. The stability of the latex was determined by the presence or not of fixed charges at the surface of the particles. The latices with particles carrying neutralized acrylic acid at high pH ( $\text{COO}^-$ ) led to homogeneous distributions, whereas the latices with acrylic acid at low pH (COOH) or without acrylic acid led to heterogeneous distributions. Our interpretation is that the stable latices present a narrow network of paths between particles at high polymer volume fraction, limiting the mobility of the surfactant, whereas in the less stable latices wider routes between flocs allow enough mobility for large aggregate formation. Thermal treatments of the dry films confirmed the strong confinement of the surfactant in the dense film structure obtained at high pH and the more open structure, allowing easier surfactant transport and oxygen penetration, observed at low pH. In order to account for the shapes of the profiles more quantitatively, a model was developed based on the diffusion of the surfactant and its transport by the drying front. It was found that the apparent diffusion coefficient of SDS micelles had to be lowered to a great extent ( $D = 10^{-13}$ – $10^{-14}$  m<sup>2</sup>/s) during drying in order to explain aggregate formation. It should be even lower ( $D = 10^{-15}$  m<sup>2</sup>/s) to interpret homogeneous surfactant profiles. These results are consistent with our hypothesis of the key importance of the surfactant mobility during drying.

## Introduction

Film formation from latices is an important industrial issue which also raises a number of fundamental questions in colloidal science.<sup>1</sup> The surfactant distribution, both near the interfaces and in the bulk of the film, has been extensively discussed in the literature since it may have a marked influence on the final properties of the films. For example, in the bulk, it increases the water permeability,<sup>2</sup> and at the film/substrate interface, a strong surfactant enrichment adversely affects adhesion.<sup>3</sup> In order to improve the film properties, it is thus important to know and even to be able to predict the surfactant distribution in a waterborne polymer film. Moreover, considering the surfactant as a molecular probe can help in understanding the drying mechanisms.

In the 1980s and 1990s, most of the published work was devoted to the investigation of the surfactant at the interfaces. Zhao et al.<sup>3</sup> and Kientz et al.<sup>4</sup> have used XPS, SIMS, and FTIR-ATR to quantify the surfactant concentration at the interfaces in layers with a maximum thickness of 2 μm. Zhao et al.<sup>3</sup> have shown that enrichment was a function of the nature of the surfactant/polymer couple and of the initial surfactant concentration in the latex. In their systems, enrichment was more pronounced at the air interface than at the substrate interface. Kientz et al.<sup>4</sup> have shown that, in the case of ionic surfactants in hydrophobic polymeric matrixes, the surfactant concentration at the interfaces was established during the drying period and only slowly evolved in the dry film. These studies were used to interpret adhesion properties of the films.

FTIR-ATR and step-scan photoacoustic FTIR (a technique allowing the investigation of the first 20 μm inside a film) were extensively used by Urban and co-workers.<sup>5</sup> They investigated many parameters influencing the surfactant distribution in the films and especially the interactions of the surfactant with the components of the latex particles. They were able to draw distribution profiles of the surfactant in its different states: without interactions with its environment, associated with the COOH groups of the particles, or associated with residual water. They found that the associated states were mainly located at the interfaces whereas the occurrence of the free state increased while penetrating inside the film. Zhao et al.<sup>6</sup> have focused their investigations on the effect of the neutralization of MAA groups at the surface of the particles on the mobility of an anionic surfactant, SDOSS. They found that, at 25% neutralization, surfactant exudation passed through a minimum whereas, at high neutralization, desorption and exudation of surfactant to the film/air interface were enhanced. More recently, SDS-containing films were studied<sup>7</sup> by the same group. It was shown that covalently or ionically cross-linking species or the presence of PVOH<sup>8</sup> have a significant effect on the surfactant migration and stratification at the film surface.

Rutherford backscattering spectrometry (RBS) is another interesting technique to investigate the surfactant distribution in dry films. It gives quantitative information about the surface enrichment in the first micrometer under the surface. Aramendia et al.<sup>9</sup> used RBS coupled with AFM to compare the surface of films stabilized with a conventional surfactant, SDS, or with a reactive surfactant (surfmer) grafted to the surface of the particles. They found, as expected, that the surface enrichment is higher with SDS and that it increased with the annealing

\* Corresponding author. E-mail: yves.holl@unistra.fr.

temperature. A particularly high enrichment is observed when the annealing temperature is above the glass transition temperature of the shell of the particles. Using the same techniques, Tzitzinou et al.<sup>10</sup> followed the evolution of the morphology of the surfactant at the surface of the films. They observed a decrease of the surface area-to-volume ratio, while the surfactant concentration remained constant, and speculated that this evolution was driven by a reduction in surface energy. RBS was also used by Lee et al.<sup>11</sup> in order to compare measured surface enrichments with those predicted by a theoretical model.<sup>12</sup>

Complete surfactant profiles, through the whole thickness of the films, could be obtained by infrared microscopy<sup>13</sup> and confocal Raman spectroscopy.<sup>14</sup> IR microscopy was used to study the evolution of the surfactant distribution in films made from poly(dimethylsiloxane) aqueous emulsions. It appeared that, after drying, the film/air interface was depleted whereas the concentration in the bulk was overall constant and a strong enrichment occurred at the substrate side. In these systems, the surfactant distribution still evolved in the dry state and a strong enrichment at both interfaces was finally observed. The authors explained the surfactant distribution by the transport of the surfactant by the drying front and also by the coalescence of the particles, both phenomena leading to heterogeneous profiles. Belaroui et al.<sup>14,15</sup> used confocal Raman spectroscopy to obtain surfactant concentration profiles through waterborne polymer films. They investigated the effect of the  $T_g$  of the acrylic core of the particles and the acrylic acid content in the shell (1 or 4%). They showed that the interfaces of the films were enriched in SDS and that the surfactant distribution in the films was rather heterogeneous. This heterogeneity has been attributed to the desorption of the surfactant as the particles get closer upon drying and its transport by water. In a more recent study, Xu et al.<sup>16,17</sup> used confocal Raman spectroscopy in complement to AFM in order to investigate the surfactant distribution in PSA films. They have shown that the enrichment at the surfaces of the film is more important with an ionic surfactant than with a nonionic surfactant, because of the better compatibility of the latter with the polymer. They could fit the concentration profiles near the interfaces by an exponential decay model. In a following study,<sup>17</sup> they investigated the effect of exposure to moisture on the surfactant concentration and organization at the surface of the films. They found that low levels of moisture led to stronger surfactant exudation. Exposing the samples to moisture cycles led to a reduction of the enrichment at both interfaces and to a more even distribution of the surfactant aggregates.

Recently, a new technique derived from confocal Raman spectroscopy has appeared: Inverse-Micro-Raman-Spectroscopy (IRMS) in which the light is focused on the sample from underneath through a transparent substrate. This technique is well suited to the investigation of latices during drying. It has been used by Ludwig et al.<sup>18</sup> to follow the water content in a drying coating. They could show that the water concentration was homogeneous through the thickness of the film until the water concentration was very low (5 wt %). On the contrary, drying was laterally inhomogeneous due to a horizontal mass flow toward the edges driven by a capillary pressure gradient.

A model, already mentioned above, was developed by Gundabala et al.<sup>12</sup> in order to predict the surfactant distribution in waterborne polymer films until the particle volume fraction reached 0.64. Based on the diffusion and convection of the particles and of the surfactant, and on the adsorption isotherms of the surfactant on the particles, the model always predicts a

surfactant enrichment at the air side. More uniform distributions of the surfactant are obtained for low surfactant Peclet numbers, in other words for high rediffusion of the surfactant.

We have seen from the numerous previous studies that the surfactant distribution in waterborne polymer films is a complex problem. It is influenced by a large number of parameters, such as the compatibility between the surfactant and the polymer, the initial surfactant concentration, the drying conditions, the neutralization of the particles carrying acid functions, etc. Thus, it would be interesting to classify the surfactant/polymer systems in categories according to the distribution of the surfactant in the resulting films.

In this paper, we describe the effects of key physicochemical parameters on the surfactant distribution in waterborne films, namely the diameter of the latex particles (30 or 100 nm),  $T_g$  of their core ( $-41$  or  $7$  °C), composition (with or without acrylic acid, with or without mineral filler), and the pH of the latex. Confocal Raman spectroscopy is the main technique used for this work. After film formation under precisely controlled conditions, the films were analyzed at different positions from the center to the edges. We found different surfactant concentration profiles for different physicochemical characteristics of the films and for different positions. Our results bring new insights into latex drying mechanisms and are consistent with a simple model that explains the formation of surfactant aggregates.

## Materials and Methods

**Latices and Films.** Two kinds of latices were used in this study: pure polymer latices and organic/inorganic composite latices, the latter provided to us by the Laboratory of Chemistry and Polymerization Processes (LCPP) in Lyon, France.

**Pure Polymer Latices.** Two core–shell latices were synthesized, differing by the composition of the particle core: either n-butyl acrylate ( $T_g = -41$  °C), or a BuA/MMA copolymer (59.5% BuA, 39.5% MMA,  $T_g = 7$  °C). The particles contained 1% acrylic acid, mainly located in the shell.<sup>15</sup> All particles had a diameter of 110 nm. The surfactant was sodium dodecyl sulfate (SDS). The polymerization was initiated by ammonium persulfate ((NH<sub>4</sub>)<sub>2</sub>S<sub>2</sub>O<sub>8</sub>). All reagents were used as received. The syntheses were performed by a semicontinuous emulsion polymerization process, in a double-wall glass reactor, under inert atmosphere. By adapting the synthesis process and using Abex 2005 (Rhodia, Inc., Cranbury, NJ) as a surfactant, a nanolatex (BuA/MMA/AA 59.5/39.5/1) with particles of 30 nm in diameter could be synthesized. More details about the synthesis can be found in ref 19.

**Composite Latices.** They were synthesized by miniemulsion, with a composition of 50% BuA and 50% MMA. The inorganic filler, laponite, was grafted at the surface of the particles. Laponite is a synthetic silicate clay, composed of platelets with a diameter of 30 nm and a thickness of 1 nm. The faces of the platelets are negatively charged whereas the edges are positively charged at a pH lower than 9. Incorporating 7% of laponite led to particles with a diameter of 165 nm, whereas the blank latex (0% laponite) had a particle diameter of 98 nm. Acrylic acid could not be introduced in composite latices. More details about the synthesis can be found in ref 20.

All latices were purified by dialysis using a Millipore membrane until the conductivity of the water in contact with the latex was less than 3  $\mu$ S/cm. Purification allows elimination of the water-soluble impurities (residual salts, oligomers, and surfactant). After purification, the solids content of the latices was adjusted to 25%, except for the nanolatex whose solids content was 15%. A 6% amount of SDS based on total solids

**TABLE 1: Composition and Characteristics of the Latices Used in This Study**

latex	composition (%BuA/%MMA/%AA)	solids content, %	mean particle diameter (nm)	pH
BuA/MMA1 110 pH 10	59.5/39.5/1	24.9	114	10
BuA/MMA1 110 pH 3	59.5/39.5/1	24.4	112	3
BuA/MMA1 30 pH 10	59.5/39.5/1	15.1	32	10
BuA1 110 pH 10	99/0/1	24.8	116	10
BuA1 110 pH 3	99/0/1	23.6	113	3
LCPP 0%	50/50/0	23.5	98	7
LCPP 7%	50/50/0 + 7% laponite	23.4	165	8

content was then postadded. The pH of the pure polymer latices was adjusted to 3 or 10 by adding either diluted hydrochloric acid or sodium hydroxide aqueous solution. The pH of the composite latices was not adjusted and remained around 8 after dialysis. The characteristics of the different latices are gathered in Table 1.

Films were prepared on quartz plates (glass could not be used because of the problem of fluorescence in Raman spectroscopy) by depositing 300  $\mu\text{L}$  of the latex with a micropipet, leading to a mean thickness of about 60  $\mu\text{m}$ . For the more diluted nanolatex, 400  $\mu\text{L}$  was deposited. The films were dried at least 10 days, and not more than 15 days, under controlled conditions (22  $^{\circ}\text{C} \pm 2$   $^{\circ}\text{C}$  and 55%  $\pm$  5% HR).

**Confocal Raman Spectroscopy.** This technique allows local analysis, in the micrometer range, of a transparent sample. Thanks to the confocal device, the investigated volume can be moved along the  $z$ -axis from the surface (air/film interface) to the film/substrate interface. It is also possible to move the sample in the plane of the film, allowing a local investigation in the  $x$ - $y$  plane.

Raman measurements were performed with a Jobin Yvon Horiba spectrometer (LABRAM BX40). Excitation at a wavelength of 632.81  $\text{cm}^{-1}$  was provided by a He–Ne laser. The diameter of the confocal pinhole was 100  $\mu\text{m}$  and a 100 $\times$  objective was used, leading to a spatial resolution of about 2  $\mu\text{m}$ . Under these conditions, with our latices, one measurement corresponded to a domain containing hundreds of particles. It is worth stressing the fact that what is called a homogeneous profile in this paper does not necessarily correspond to the surfactant still homogeneously distributed around the initial latex particles. Aggregates smaller than the resolution of the microscope could also exist. For each point, 8–10 spectra were accumulated during 120 s, leading to a satisfying signal-to-noise ratio. Raman spectroscopy can be used for quantitative analysis since the Raman signal is known to be proportional to the concentration. Thus, the surfactant concentration can be measured in the films after a preliminary calibration. By plotting the intensity of one SDS peak ( $\text{S}=\text{O}$  peak at 1086  $\text{cm}^{-1}$ ) relative to one polymer peak ( $\text{C}-\text{C}$  at 1063  $\text{cm}^{-1}$ ) as a function of SDS concentration, a calibration curve (straight line) was obtained. The sulfate contribution from the initiator was negligible because the corresponding peak was not detectable in the surfactant-free films.

Our films were analyzed along the vertical  $z$ -axis at different  $x$ - $y$  positions, as represented in Figure 1. Profiles were obtained, giving the SDS concentration as a function of the depth in the film. From these profiles, it was possible to calculate the mean and standard deviation of the surfactant concentration. Since a marked surface enrichment has a strong influence on the standard deviation but not on the average, the surface concentration was not taken into account for the calculation of the standard deviation. The films are divided into three different zones: 1 = the center of the film; 2 = an intermediate position between the center and the edge; 3 = the edge of the film. The center

corresponds to the geometric center of the film ( $X = 0$ ;  $Y = 0$ ). The limit between zones 2 and 3 is situated at 2/3 of the radial distance from the geometric center to the edge. Profiles obtained very close to the edge of the films were not taken into account in the correlation diagrams. Correlation diagrams are obtained by plotting the average concentration and its standard deviation as a function of the position (1, 2, or 3) in the film (see Figure 2 as an example).

## Results

**Pure Polymer Latices.** The effects of the size of the particles, their composition, and the pH of the latex were investigated. Figure 1 presents the profiles obtained at different points (numbered 1 to 5) in a BuA/MMA1 110 nm pH 10 film. All points present a homogeneous distribution of the surfactant through the thickness of the film. The surface is enriched with surfactant. The correlation diagram (Figure 2) shows that the average surfactant concentration is the same whatever the position (slightly above 6%). The low standard deviation of the SDS concentration through the film reflects its homogeneous distribution.

Two profiles obtained in a film made from the nanolatex are presented in Figure 3. The composition of the particles and the pH of the latex are the same as those in the previous case, but the particles are three times smaller. Again, the surfactant distribution is homogeneous throughout the film, as shown in the profiles and on the correlation diagrams (Figure 4). In this case, the surface of the film is not enriched and the average SDS concentration is close to 6%.

By considering a particular, but representative, profile (Figure 5), one can notice that the surface of the films made from soft particles (BuA1) with a diameter of 110 nm at pH 10 is strongly enriched. This enrichment is followed by a depletion zone, itself followed by a zone with an oscillating surfactant concentration around 6%. Through the thickness, a quite homogeneous distribution of the surfactant is observed. These films present a mean concentration slightly above 6% and a weak increase of the concentration from the center to the edge (Figure 6). The standard deviation is low but still slightly higher than in the case of the copolymer (Figure 2).

Changing the pH of the initial latex, from 10 to 3, has a dramatic effect on the surfactant distribution through the films (Figures 7–10). Variations in the surfactant concentration through the films are observed, representative of surfactant aggregates, as already observed by Belaroui et al.<sup>15</sup> The amplitude and the frequency of the oscillations are not constant and it can be observed, from the correlation diagrams of the standard deviation (Figure 8 and Figure 10), that the SDS distribution is more heterogeneous near the edge (higher standard deviation). In both cases, the average SDS concentration is higher at the center of the film and decreases near the edges.

Another particle composition was also investigated, namely BuA/MMA 50/50 without acrylic acid (Figure 11 and Figure

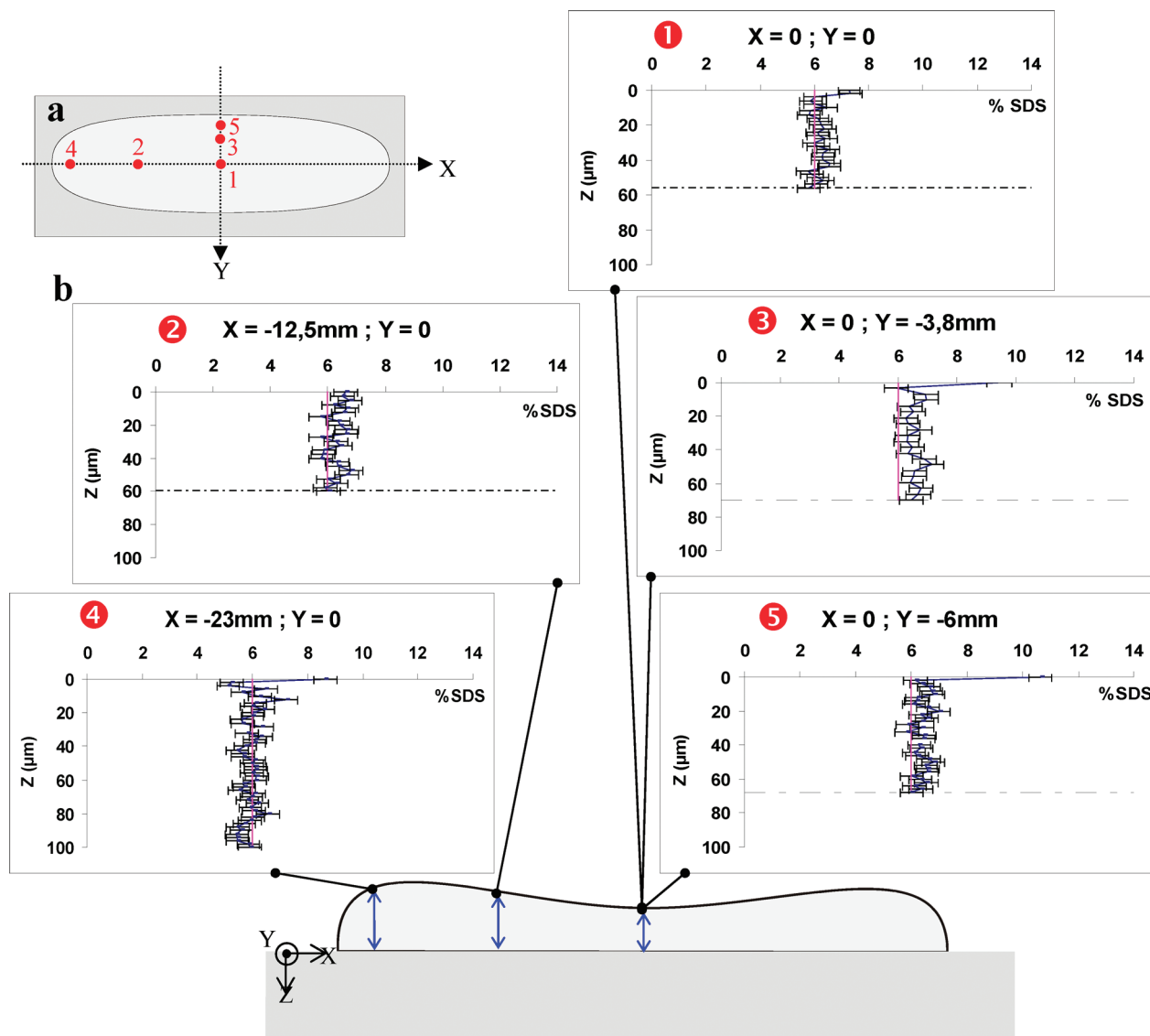


**Figure 1.** (a) Top view of a BuA/MMA1 110 nm pH10 + 6% SDS film with the positions of the presented profiles. (b) Side view of the film and SDS concentration profiles.

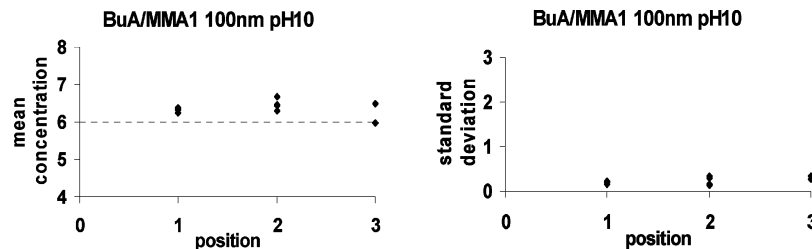


**Figure 2.** Correlation diagrams of the SDS mean concentration (left) and the standard deviation (right) calculated from the SDS concentration profiles in BuA/MMA1 110 nm pH 10 + 6% SDS films.

12). This latex corresponds to the blank reference synthesized at LCPP (LCCP 0%, see Table 1). The profile and the correlation diagrams clearly show that the surfactant distribution is heterogeneous, with a mean surfactant concentration through the films close to 6% whatever the analyzed point. The standard deviation is also constant from the center to the edge of the film, meaning that variations in the surfactant distribution do not depend on the analyzed zone.

From these results, it seems that the pH and the presence of acrylic acid have a strong influence on the surfactant distribution. Their effect is demonstrated in the correlation diagrams gathered

in Figure 13 and Figure 14. At pH 10, varying the size or the composition of the particles has almost no effect on the bulk surfactant distribution and only a slight effect on the surface enrichment. Decreasing the size of the particles cancels the surface enrichment, whereas soft particles lead to a strong enrichment. Surface enrichment will be specifically discussed in a following paper.<sup>21</sup> Decreasing the pH or removing the acrylic acid leads to high standard deviations. Two kinds of surfactant distributions can thus be observed: the heterogeneous distributions at pH 3 or without acrylic acid and the homogeneous distributions at pH 10.

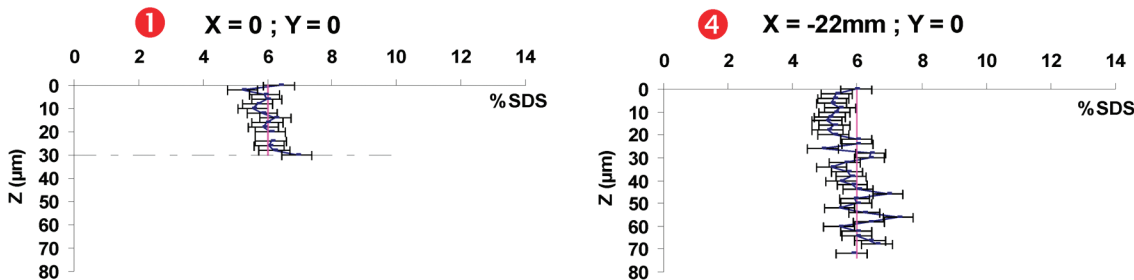


**Figure 3.** Representative examples of SDS concentration profiles in a BuA/MMA1 30 nm pH 10 + 6% SDS film. The positions of the profiles are indicated by the red numbers on the graphs and refer to the positions given on the sketch in Figure 1a.

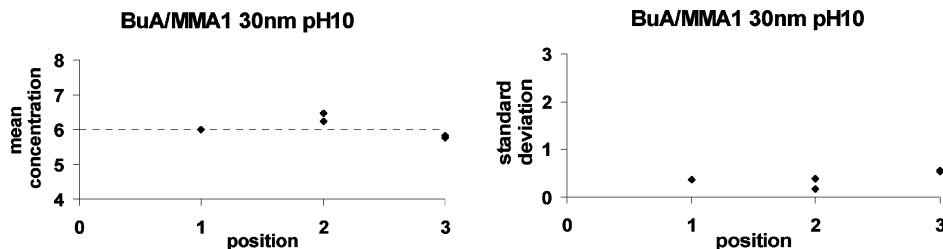


**Figure 4.** Correlation diagrams of the SDS mean concentration (left) and the standard deviation (right) calculated from the SDS concentration profiles in a BuA/MMA1 30 nm pH 10 + 6% SDS film.

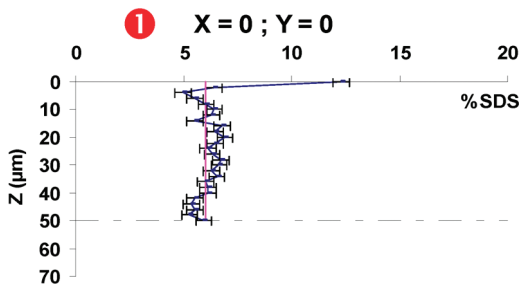


**Figure 5.** Representative example of SDS concentration profiles in a BuA1 110 nm pH 10 + 6% SDS film. The position of the profile is indicated by the red number on the graph and refers to the position given on the sketch in Figure 1a.

**Composite Latex.** The results concerning the surfactant distribution in the films made from the composite latex are presented in Figures 15 and 16. The profiles obtained in the central part of the film are homogeneous whereas large variations of the SDS concentration are observed near the edges. This particular result is made clearer by the correlation diagrams with the increase of the standard deviation from the center to the edge. The correlation diagram of the mean concentration shows that this value remains constant from the center to the edge of the film.

**Thermal Treatments.** Two BuA/MMA1 110 nm + 6% SDS films, at pH 10 and pH 3, were submitted to thermal treatments: 75 °C during 90 min or 75 °C under reduced pressure (~1 Pa) during 11 days (the reduced pressure was expected to reduce SDS oxidation). These films were chosen because the surfactant distribution was homogeneous in the first one whereas the second one presented aggregates.

During thermal treatment of the films, pure SDS powder was also submitted to the same treatment in order to gain information about a possible degradation of the surfactant. The Raman spectra of the pure surfactant before and after thermal treatments are presented in Figure 17. The shorter thermal treatment, 75 °C during 90 min, had no significant effect on the SDS spectrum whereas the longer one markedly affected it. Some peaks disappeared at 1296, 1230, 838 cm<sup>-1</sup>, and the SO<sub>4</sub> peak at 1086 cm<sup>-1</sup>, used to quantify the SDS concentration, was almost

absent. Simultaneously, new peaks appeared at 1042 and 1002 cm<sup>-1</sup>, probably due to SDS degradation products.

Films from BuA/MMA1 110 nm + 6% SDS at pH 10 were analyzed after the two thermal treatments. The SDS profiles presented in Figure 18 and Figure 19 were respectively obtained after 90 min at 75 °C and 11 days at 75 °C under reduced pressure. These profiles were measured at the center of the films, but they were representative of the results obtained at other points. Both thermal treatments had no effect on the distribution of the surfactant since the profiles were similar to those obtained before thermal treatment (Figure 1b).

Films prepared from BuA/MMA1 110 nm + 6% SDS at pH 3 were also investigated after thermal treatment. After 90 min at 75 °C, the profile obtained in the central part is presented in Figure 20. In this zone, the surfactant distribution is not modified by the thermal treatment since it is comparable to the profile no. 1 in Figure 7b (same film without treatment). One representative profile obtained in the peripheral part of the film is presented in Figure 21. In this zone, the surfactant distribution was significantly influenced by the thermal treatment. First, the profile is centered at 2% SDS instead of 6%. Then, an aggregate is observed at about 15 μm from the air/film interface. This was systematically found in all reproducibility checks. Finally, one can notice that the point corresponding to the film/air interface is absent from the profile: the surface concentration could not be calculated from the spectrum of the surface (Figure 22) because the peak at 1086 cm<sup>-1</sup> had a very low intensity and around 1030 cm<sup>-1</sup> the shape of the peak was much enlarged. This prevented us from using our previous calibration.

In a last step, a BuA/MMA1 pH 3 film was submitted to a thermal treatment at 75 °C during 11 days under reduced pressure. No profiles could be obtained from this sample in any zone of the film because the SDS concentration could not be calculated. The S–O peak at 1086 cm<sup>-1</sup> was always absent from all spectra, and at the surface, the spectra were deformed in the same way as previously (Figure 22).

## Discussion

The surfactant concentration profiles in the films can be classified in two main categories: homogeneous or heteroge-

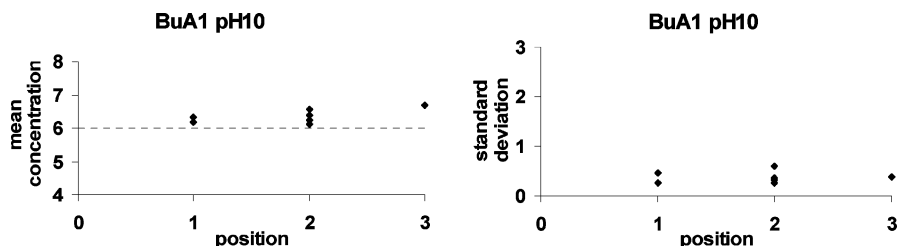


**Figure 6.** Correlation diagrams of the SDS mean concentration (left) and the standard deviation (right) calculated from the SDS concentration profiles in BuA1 110 nm pH 10 + 6% SDS films.

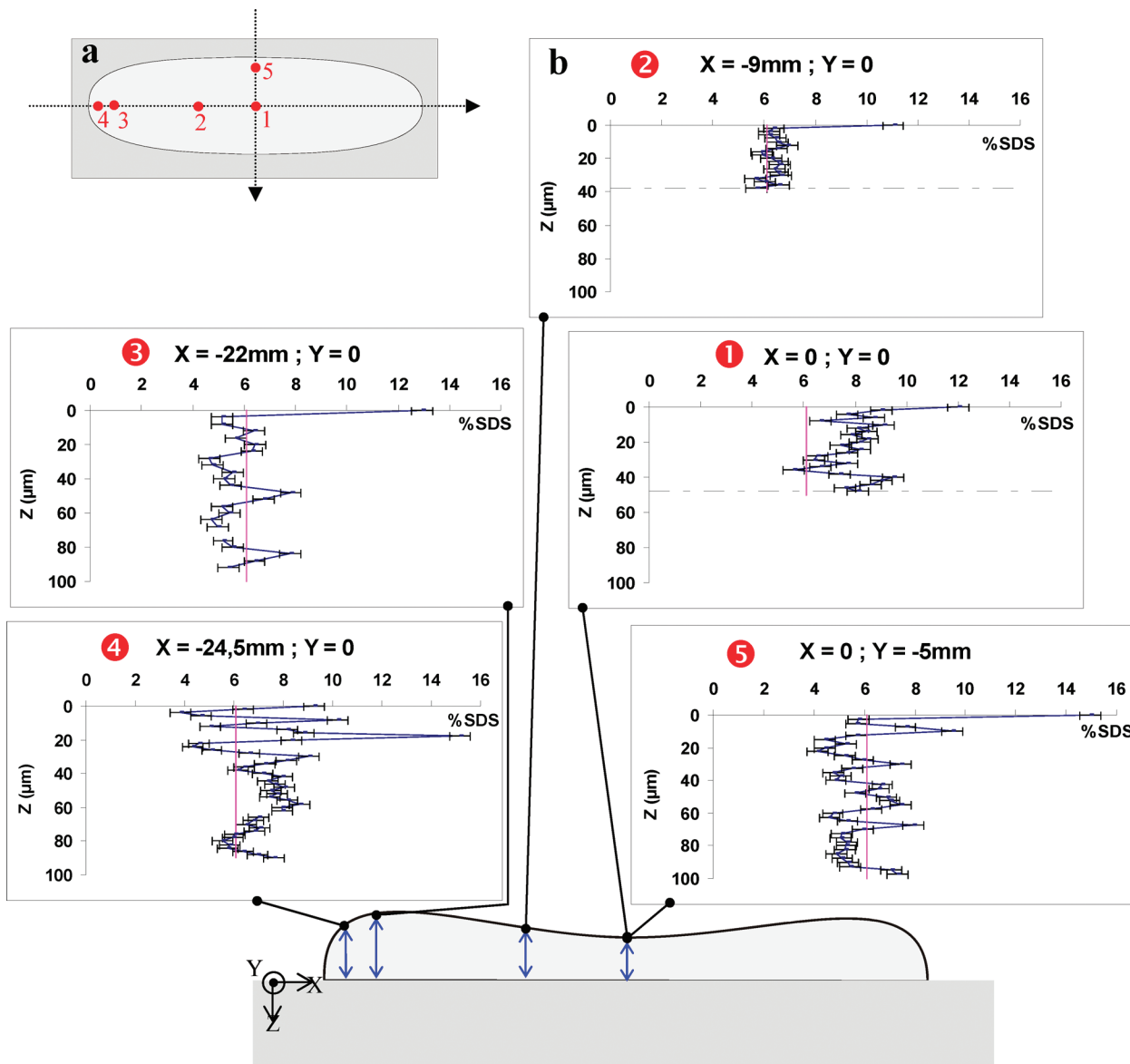


**Figure 7.** (a) Top view of a BuA/MMA1 110 nm pH 3 + 6% SDS film with the positions of the presented profiles. (b) Side view of the film and SDS concentration profiles.

neous. The homogeneous distribution of the surfactant is observed in films made from latices containing acrylic acid at pH 10. A high pH creates a strong electrostatic stabilization owing to the carboxylate functions ( $\text{COO}^-$ ) in addition to the stabilization brought by the anionic surfactant. A mechanism for the formation of homogeneous profiles is proposed in Figure 23. The high stability of the latex allows the particles to get closer and deform during drying without making contact. The surfactant can diffuse throughout the film between the particles and remain homogeneously distributed during most of the drying

process. It is only at the very end of drying that particles come into contact (either through the whole film as represented in Figure 23 or along a gradient from the air toward the substrate), suddenly decreasing the surfactant mobility and entrapping it between the particles. In this case, the final drying front is not able to drive the surfactant over significant distances. As a result, the surfactant distribution appears homogeneous on a micrometer scale in confocal Raman analysis.

This kind of homogeneous profile is similar to those observed by Xu et al.<sup>16</sup> They used particles with a comparable composi-

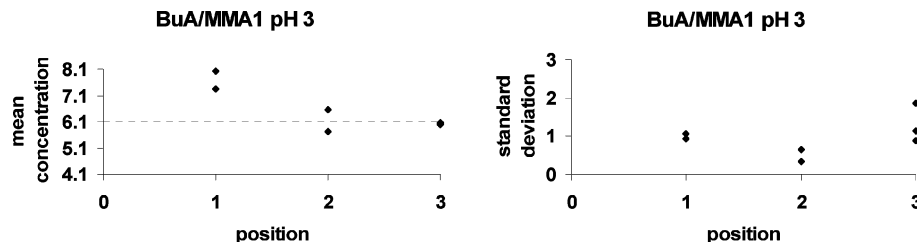


**Figure 8.** Correlation diagrams of the SDS mean concentration (left) and the standard deviation (right) calculated from the SDS concentration profiles in BuA/MMA1 110 nm pH 3 + 6% SDS films.

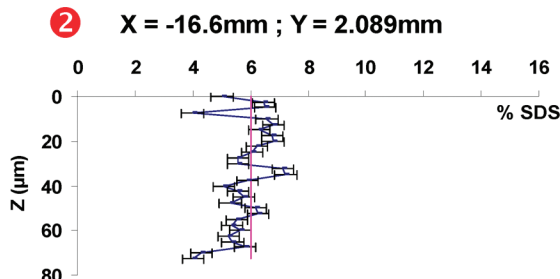


**Figure 9.** Representative example of SDS concentration profiles in a BuA1 110 nm pH 3 + 6% SDS film. The position of the profile is indicated by the red number on the graph and refers to the position given on the sketch in Figure 1a.

tion (n-butyl acrylate, vinyl acetate, and methacrylic acid) stabilized with an anionic surfactant. Their profiles present a slight surface enrichment and a constant concentration in the bulk. The lower surface enrichment may be explained by the lower concentration in the initial latex. Connecting the homogeneous distribution of the surfactant in the bulk to the surface charges of the particles is difficult in this case. The pH of their initial latex is close to the  $pK_a$  of methacrylic acid, leading to a lower surface charge than in our case. It should also be noted that, in the bulk, fewer measurements were performed, thus possibly leaving some aggregates undetected.

Heterogeneous profiles were obtained with acrylic acid at low pH or without acrylic acid. These latices are mainly stabilized by the ionic charges carried by the surfactant. This weaker stabilization allows particle flocculation (Figure 24). Between flocs, wide paths allow the circulation and redistribution of the surfactant. As the drying front passes through the film, the surfactant is swept and accumulates at the air/water interface. This interface gets enriched and the viscosity increases. Above a certain concentration, the surfactant is deposited and forms aggregates at a certain level in the film. The drying front then goes deeper, sweeping surfactant again until new aggregates are deposited at a lower level. This could explain the oscillatory surfactant concentration along the  $z$  direction. A recent study by Gauer et al.<sup>22</sup> clearly confirms that charges fixed at the particle surface more efficiently prevent aggregation and coalescence than mobile charges of adsorbed ionic surfactants.

In the case of the latex containing 7% laponite, the two kinds of profiles, homogeneous at the center and heterogeneous at the edges, were observed (Figure 15 and Figure 16). Why two types of profiles can coexist on the same film is not clear. Following our interpretation presented above, it seems that at the edge of the film, where drying rapidly starts, the colloidal stability is low whereas in the center, where drying is slower, the system gets more stable. More work is required to better explain this behavior.

The effect of thermal treatment on the distribution of SDS in BuA/MMA1 110 nm + 6% SDS films has been investigated (Figures 18–21). In the case of the homogeneous distribution

(pH 10), we expected an evolution of the concentration profile, as often reported in the literature,<sup>9,23,24</sup> toward a detectable phase separation (aggregate formation), as SDS is highly incompatible with the acrylic polymers. This was not observed. The homogeneous distribution remained remarkably stable, at the investigated scale (at a scale lower than a micrometer, reorganization of the surfactant may occur without being detected by confocal Raman spectroscopy), even after 11 days at 75 °C (Figure 19). SDS seems highly confined at the interfaces between particles, possibly in the form of nanometric aggregates. High confinement also protects SDS from oxidative degradation. Protection also takes place at the film surface where the surfactant is more exposed to air, which is surprising. These facts can be seen as a confirmation of our hypothesis of a dense, probably ordered, packing of latex particles at pH 10.

At pH 3, the situation is different. After the short treatment (90 min) at 75 °C, the center of the film is not affected (Figure 20) but, in the edge region (Figure 21), SDS massively migrates toward the surface where it is degraded. This stresses once more the differences between the center and the edge of the film, such as in the case of the composite latex (Figure 15), which probably reflect different drying mechanisms. The long treatment (11 days), even under reduced pressure, totally degrades SDS all over the film. An immediate interpretation is to invoke both acidic conditions and a more open film structure, also in line with our previously proposed mechanism.

In summary, we have seen that before thermal treatment the pH has an influence on the final SDS distribution in the films. After thermal treatment, the structure of the film leads to variable effects on the surfactant distribution. Strong confinement at pH 10 prevents migration and degradation of SDS. A more open structure and an acidic environment lead to both migration and degradation of SDS. Scalarone et al.<sup>24</sup> investigated the effect of a thermal treatment on the surfactant contained in a waterborne polymer film. By the combined use of ATR-FTIR and AFM, clear evidence of thermal degradation of SDS was provided. Even if the conditions were more severe (120 °C, 500 h), these observations are in line with ours. Their results also indicated that the surfactant contained in a film underwent a slower degradation than the pure surfactant submitted to thermal treatment. They attributed this fact to the lower oxygen concentration and availability inside the film and also to the low diffusion coefficient of the surfactant toward the film surface. Patterson et al.<sup>25</sup> showed that even more drastic conditions (700 °C) resulted in a 65% weight loss of SDS, the degradation products consisting of alkenes, primary alcohols, and ethers (such as didodecyl ether).

**Model for Aggregate Formation.** Routh and coworkers<sup>12</sup> developed a consistent theoretical framework to understand surfactant distribution in latex films. These authors considered a drying latex, starting in a dilute state, until the particle volume fraction reached 0.64 (disordered close packing of monodisperse spheres). The model is based on convection and diffusion of

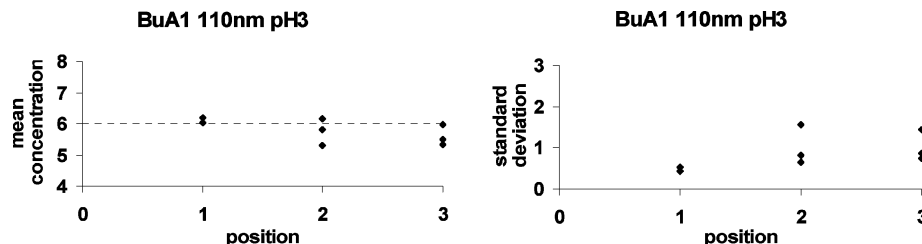


**Figure 10.** Correlation diagrams of the SDS mean concentration (left) and the standard deviation (right) calculated from the SDS concentration profiles in BuA1 110 nm pH 3 + 6% SDS films.

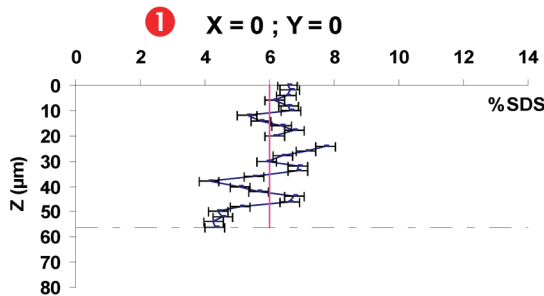


**Figure 11.** Representative example of SDS concentration profiles in a LCPP 0% pH 8 + 6% SDS film. The position of the profile is indicated by the red number on the graph and refers to the position given on the sketch in Figure 1a.

surfactant and particles during drying, and on the adsorption isotherm of the surfactant on the particles. The distribution of the particles through the film is controlled by the particle Peclet number ( $Pe$ ), defined by the relative importance of the convection and diffusion mechanisms. The evaporation rate is assumed to be constant and the particles, initially unsaturated, can adsorb surfactant during latex concentration. The particle Peclet number is always higher than 1, meaning that they accumulate at the water/air interface. The surfactant Peclet number is variable. The model predicts that when the surfactant easily rediffuses in water ( $Pe < 1$ ), its final distribution will be rather homogeneous in the film. On the other hand, with a surfactant Peclet number fixed at 1, the distribution of the surfactant is a function of the plateau level and the slope of the Langmuir isotherm. Increasing these two parameters leads to strong film/air surface enrichment. The model does not predict completely homogeneous distributions of the surfactant because the particles are not initially saturated. Moreover, it does not allow aggregate formation until close packing of the particles but rather it predicts parabolic profiles. Aggregate formation seems to be only possible in the last stages of drying, in highly concentrated systems.

In the model we developed, the particles are initially close-packed ( $\Phi = 0.64$ ) and drying proceeds until total evaporation of water. The surfactant is initially homogeneously distributed with saturated particles and free surfactant molecules and micelles in water. Some assumptions are made: lateral drying fronts are neglected, the drying rate is constant, and the surfactant diffusion coefficient is constant. As water evaporates, a drying front moves through the close-packed particles and the surfactant either diffuses in water or accumulates at the air/water interface (Figure 25).

The surfactant concentration in the film is given as a function of the position  $z$ . The position of the drying front  $z_0$ , which moves at a constant speed  $v$  corresponding to the evaporation rate of the water, is given by  $z_0(t) = vt$ . Figure 26 presents the surfactant distribution through the film initially and after a certain time  $t$ . It shows that initially,  $C(z, t = 0) = C_0$  for  $z \geq$

0 and  $C(z, t = 0) = 0$  for  $z < 0$ . At a given time  $t$ , surfactant has accumulated at the drying front and the concentration profile follows a function  $f$ ; thus, we have  $C(z, t \geq 0) = f(z, t)$  for  $z \geq vt$  and  $C(z, t \geq 0) = 0$  for  $z < vt$  because no surfactant can pass through the drying front.

Placing the origin at the air/water interface by defining a new variable  $y$  ( $y = z - vt$ ) leads to the following equations  $C(y < 0, t) = 0$  and  $C(y \rightarrow \infty, t) = C_0$ .

Applying Fick's law to our problem, with  $D$  the diffusion coefficient, we obtain eq 1 as a function of  $t$  and  $y$ :

$$\frac{\partial C}{\partial t} + \frac{\partial}{\partial y} \left( -vC - D \frac{\partial C}{\partial y} \right) = 0 \quad (1)$$

The boundary conditions are defined in eqs 2 and 3. The first expresses the fact that there is no flow across the wall and the second gives the surface excess at the time  $t$ :

$$-vC_0(0, t) - D \frac{\partial C(0, t)}{\partial y} \Big|_{y=0} = 0 \quad (2)$$

$$\Gamma = \int_0^\infty [C(y, t) - C_0] dy = C_0 v t \quad (3)$$

After solving eq 1 in the Laplace space, the surfactant concentration at the drying front is given by eq 4.

$$\bar{C} = C_0 \left( \frac{1}{s} + \frac{2}{s(\sqrt{1 + \tau_0 s} - 1)} \exp \left( -\frac{y}{\bar{y}} (1 + \sqrt{1 + \tau_0 s}) \right) \right) \quad (4)$$

with  $\tau_0 = 4D/v^2$  a characteristic time and  $\bar{y} = 2D/v$  a characteristic length of the surfactant accumulation at the air/water interface.

At  $y = 0$ ,  $\bar{C}$  simplifies to

$$\bar{C} = C_0 \left( \frac{1}{s} + \frac{2}{s(\sqrt{1 + \tau_0 s} - 1)} \right) \quad (5)$$

The inverted Laplace transform of  $\bar{C}$  then becomes:

$$C(y = 0, t) = C_0(1 + g(t)) \quad (6)$$

with

$$g(t) = \frac{e^{-t\sqrt{t}}}{\sqrt{\pi}} + t + \left( t + \frac{1}{2} \right) \operatorname{erf}\sqrt{t} \quad (7)$$

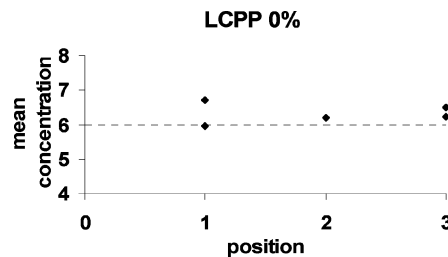


**Figure 12.** Correlation diagrams of the SDS mean concentration (left) and the standard deviation (right) calculated from the SDS concentration profiles in LCPP 0% pH 8 + 6% SDS films.

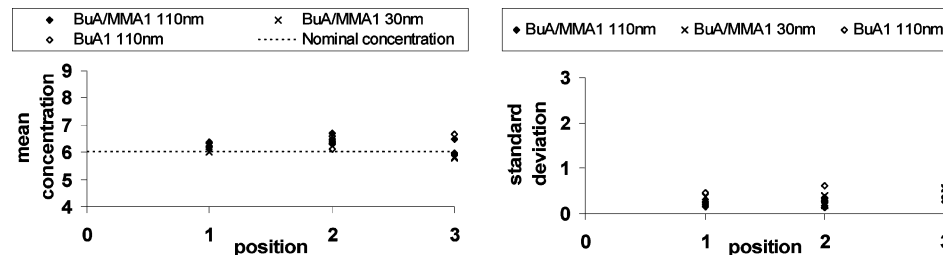


**Figure 13.** Correlation diagrams of the SDS mean concentration (left) and the standard deviation (right) calculated from the SDS concentration profiles in the films containing acrylic acid at pH 10 (superimposition of the diagrams already presented in Figures 2, 4 and 6).

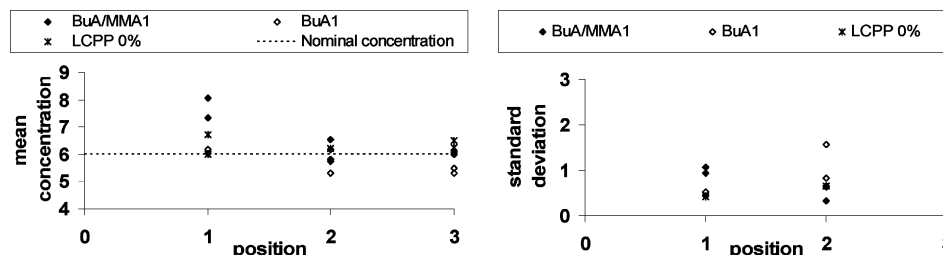


**Figure 14.** Correlation diagrams of the SDS mean concentration (left) and the standard deviation (right) calculated from the SDS concentration profiles in films containing no acrylic acid or with acrylic acid at low pH (superimposition of the diagrams already presented in Figures 8, 10, 12).

In eqs 6 and 7,  $y$  and  $t$  are relative to the characteristic time and length defined above.

Equation 6 allows us to plot the surfactant concentration  $C$ , or surfactant volume fraction  $\Phi$ , as a function of the drying time. Since the position  $z_0$  of the drying front is linked to the time by  $z_0 = vt$ , it is finally possible to plot the surfactant volume fraction  $\Phi$  at the drying front as a function of the position of the drying front  $z_0$ . The diffusion coefficient of the surfactant micelles was calculated with Stokes–Einstein’s equation according to the method described by Carlsson et al.<sup>26</sup> and was found equal to  $D = 10^{-10} \text{ m}^2/\text{s}$ . The initial surfactant volume fraction was calculated from adsorption isotherms determined by a conductometric method.<sup>19</sup> Considering a latex that leads to heterogeneous surfactant distributions, BuA/MMA1 110 nm pH 3, the calculated initial volume fraction in micelles is equal to  $\Phi_0 = 0.028$ . Since we are well above the CMC, we only consider the micelles for the calculation of the diffusion coefficient and the initial surfactant volume fraction. The evaporation rate was measured by magnetic resonance profiling<sup>19,27</sup> and was found equal to  $v = 5 \times 10^{-8} \text{ m/s}$ . The corresponding curve is shown in black in Figure 27: the surfactant volume fraction  $\Phi$  at the drying front (water/air interface) is given as a function of the position  $z_0$  of the drying front.

We considered in Figure 24 that aggregate formation was possible if the drying front gets saturated in surfactant and deposits this excess as aggregates. Saturation of the drying front is equivalent to a very high concentration and viscosity which prevents further transport of surfactant. Our hypothesis is that aggregates are formed when the viscosity of the drying front

diverges, which corresponds to a surfactant volume fraction at the air/water interface equal to 0.64. It is clear from Figure 27 that this value is never reached for a diffusion coefficient of  $10^{-10} \text{ m}^2/\text{s}$ , because rediffusion is too prominent. These parameters would lead to the transport of all the surfactant through the whole thickness of the films.

Lower diffusion coefficients have thus been tested. Figure 27 shows that for diffusion coefficients lower than  $10^{-13} \text{ m}^2/\text{s}$ , it is possible to form aggregates. For  $D = 10^{-13}$  and  $10^{-14} \text{ m}^2/\text{s}$ , surfactant is deposited as the drying front reaches a position of 22 and 5  $\mu\text{m}$ , respectively. This is good agreement with the distance observed on the experimental profiles that present aggregates, though the distance between aggregates is not found to be constant. For example, near the edge of the film made from BuA/MMA1 110 nm pH 3, the aggregates are separated by about 5–10  $\mu\text{m}$  whereas in the film made from LCPP 7%, they are separated by about 10–20  $\mu\text{m}$ . According to our model, aggregate formation is possible if the diffusion coefficient is decreased by factors of  $10^3$  to  $10^4$ . The decrease of  $D$  has already been observed with water in confined space by Doumenc et al.<sup>28</sup> In their study based on gravimetric measurements coupled with modeling of drying kinetics, they found that in concentrated systems, the diffusion coefficient of water decreases by a factor of  $10^4$ . In our case of surfactant accumulating at the drying front, the diffusion coefficient, inversely proportional to the viscosity, is also expected to decrease as the viscosity of the surfactant solution increases.

For  $D = 10^{-15} \text{ m}^2/\text{s}$ , aggregates form after a displacement of 1  $\mu\text{m}$  of the drying front. This means that such aggregates are

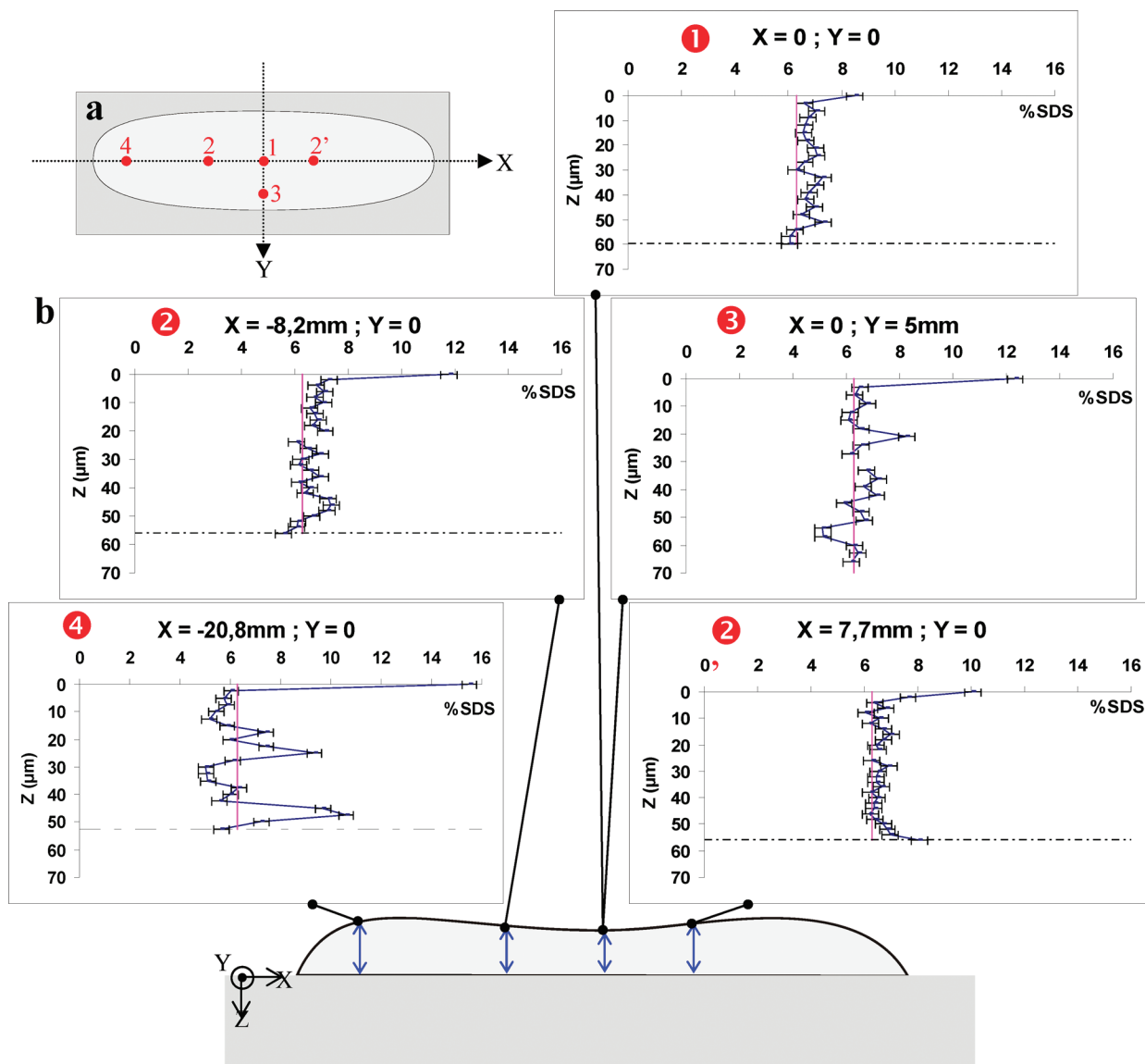


**Figure 15.** (a) Top view of a LCPP 7% pH 8 + 6% SDS film with the positions of the presented profiles. (b) Side view of the film and SDS concentration profiles.

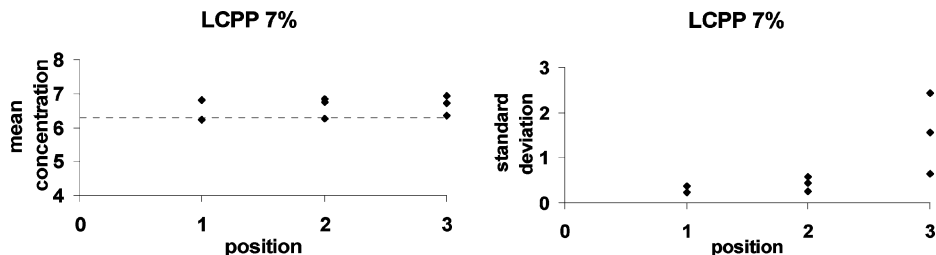


**Figure 16.** Correlation diagrams of the SDS mean concentration (left) and the standard deviation (right) calculated from the SDS concentration profiles in LCPP 7% pH 8 + 6% SDS films.

not visible by confocal Raman spectroscopy because the resolution of the technique is in the range of  $1 \mu\text{m}$ . The resulting profiles will thus present no surfactant aggregates but rather a homogeneous distribution of the surfactant. This kind of profile was observed with the latices stabilized with fixed electrostatic charges ( $\text{COO}^-$ ). We saw in Figure 23 that before the drying front passes through the particles, the surfactant is confined in a network of narrow paths. This high confinement may explain the very low diffusion coefficient of the surfactant. In these latices, the surfactant is thus transported by the drying front but on a distance that is so short that it does not have enough

time to get concentrated. Consequently, the “aggregates” formed have a concentration very close to 6% SDS and are not detected by techniques with a micrometric resolution.

Our model allows us to explain surfactant aggregate formation through an important decrease of the diffusion coefficient. This decrease is coherent with the mechanisms that we proposed previously. In a stable system, stabilized with fixed electrostatic charges, confinement is high. Thus, the diffusion coefficient will be lower than in the less stable systems. It is then coherent that the drying front gets saturated earlier with the more stable

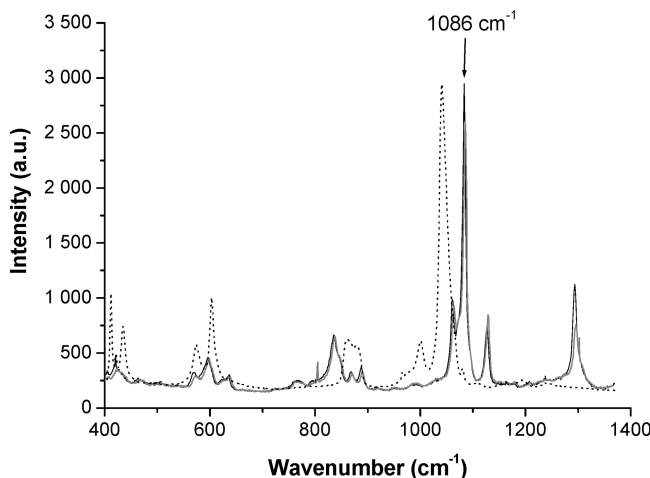


**Figure 17.** Pure SDS spectra before thermal treatment (black solid line); after 90 min at 75 °C (gray solid line); after 11 days at 75 °C under reduced pressure (black dotted line).

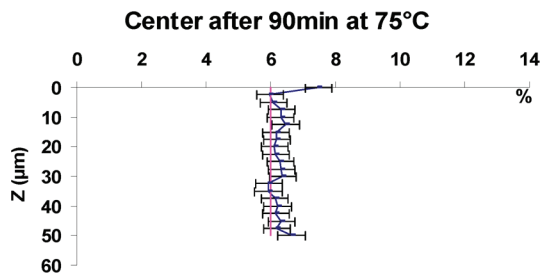


**Figure 18.** SDS concentration profile in a BuA/MMA1 110 nm pH 10 + 6% SDS film after thermal treatment at 75 °C during 90 min.

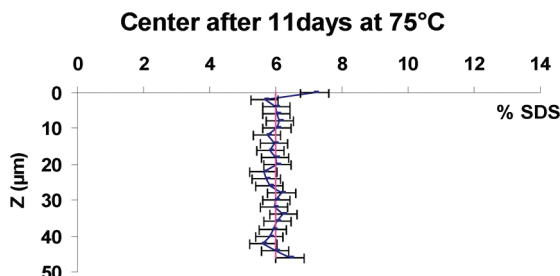


**Figure 19.** SDS concentration profile in a BuA/MMA1 110 nm pH 10 + 6% SDS film after thermal treatment at 75 °C under reduced pressure during 11 days.

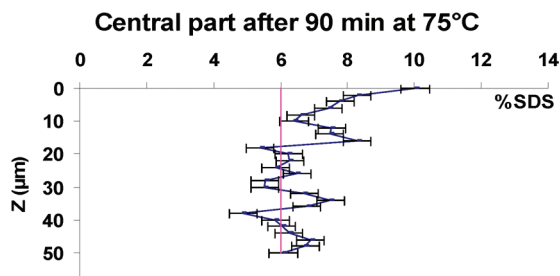


**Figure 20.** SDS concentration profile in the central part of a BuA/MMA1 110 nm pH 3 + 6% SDS film after thermal treatment at 75 °C during 90 min.

systems, leading to an apparent homogeneous distribution of the surfactant.

## Conclusion

We have shown that the presence of fixed electrostatic charges at the surface of the latex particles leads to a homogeneous

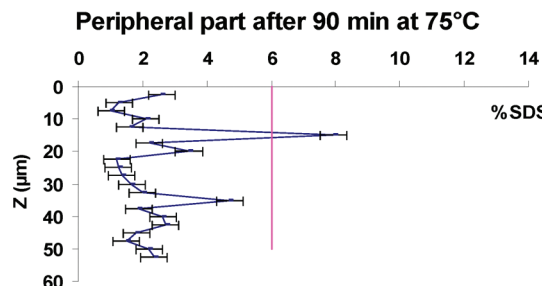


**Figure 21.** SDS concentration profile in the peripheral part of a BuA/MMA1 110 nm pH 3 + 6% SDS film after thermal treatment at 75 °C during 90 min.

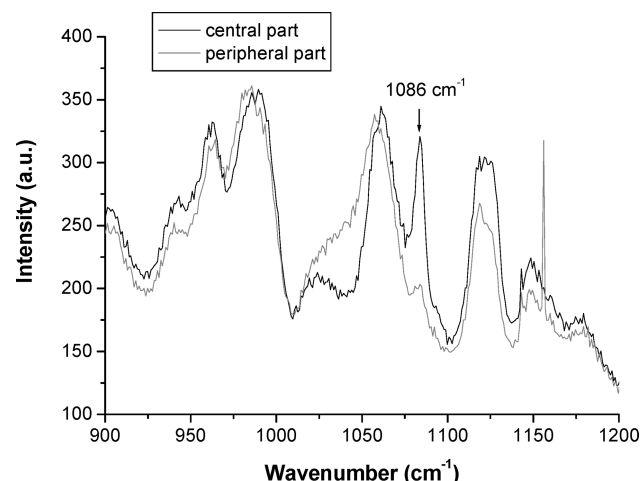


**Figure 22.** Spectra obtained at the surface of a BuA/MMA1 110 nm pH 3 + 6% SDS film after 90 min at 75 °C in the central part (black line) and in the peripheral part (gray line).

surfactant distribution in the dry films. This distribution is left unchanged after thermal treatments. Particles without acrylic

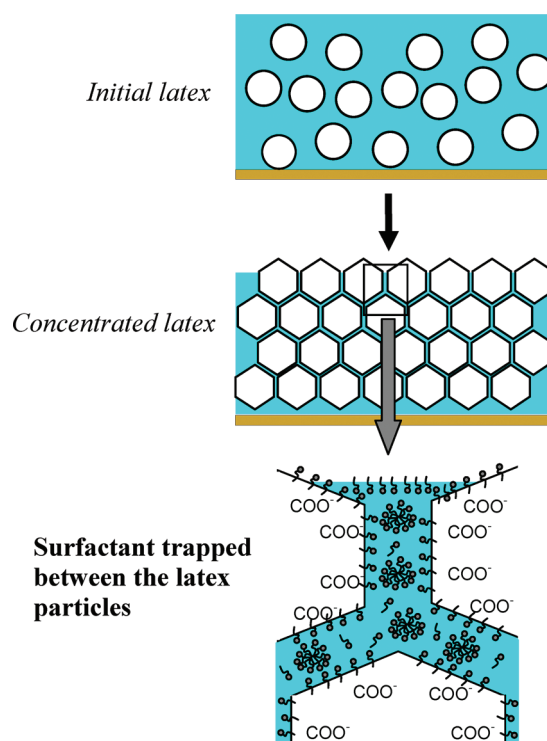


**Figure 23.** Sketch of the film formation process from a highly stabilized basic latex. An abrupt decrease in surfactant mobility at the end of drying entraps it in the interparticle space.

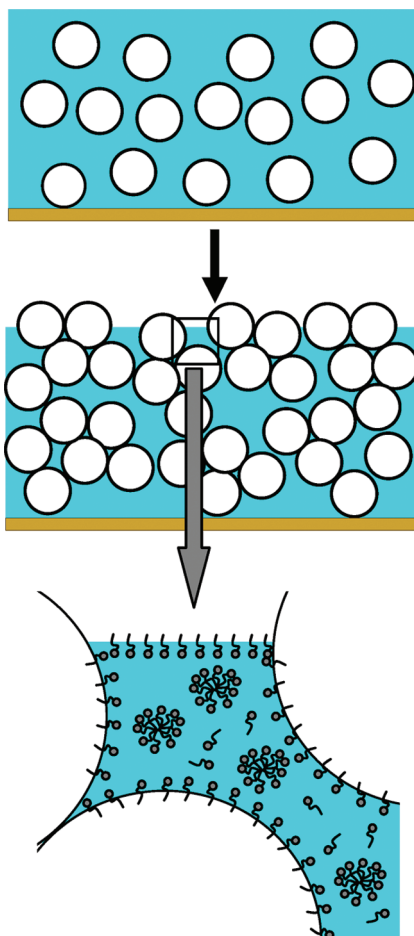


**Figure 24.** Sketch of the film formation process from a latex carrying no fixed electrostatic charges. The dispersion is less stable than in the previous case (Figure 23), leaving a more open structure in which the drying front is able to sweep the surfactant until it forms micrometer-sized aggregates.

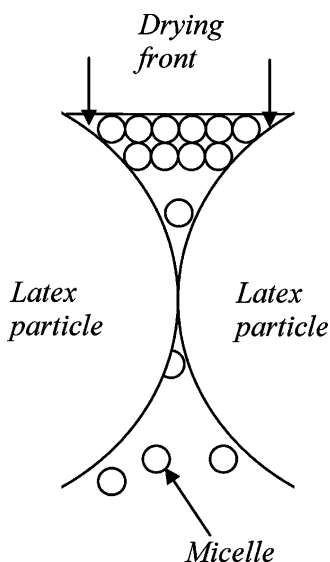


**Figure 25.** Evolution of the drying front through the close-packed particles. The surfactant, here in micelles, either rediffuses in water or accumulates at the air/water interface.

acid or at an acidic pH led to the formation of surfactant aggregates in the final films. The model that we developed, based on the diffusion and transport of the surfactant during drying, confirms the mechanisms proposed to explain the shape of the surfactant profiles.

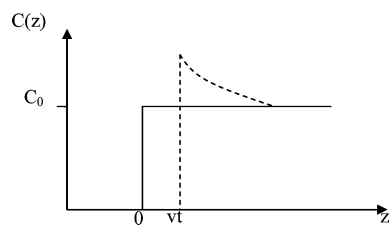


**Figure 26.** Schematic plot of the surfactant concentration  $C(z)$  as a function of the position  $z$  in the film, initially at close packing (—) and after a time  $t$  (---).

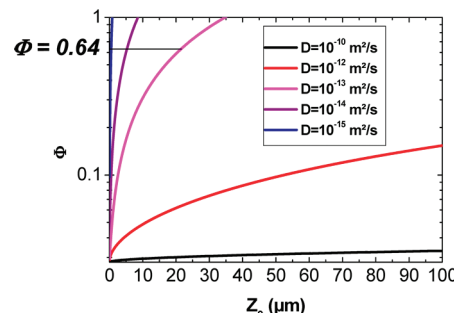


**Figure 27.** Surfactant volume fraction  $\Phi$  at the drying front as a function of the position  $z_0$  of the drying front in the film for  $D = 10^{-10}$  (black),  $10^{-12}$  (red),  $10^{-13}$  (pink),  $10^{-14}$  (purple),  $10^{-15}$  (blue)  $\text{m}^2/\text{s}$ ,  $\Phi_0 = 0.028$  and  $v = 5 \times 10^{-8} \text{ m/s}$ . The  $z$ -range covers  $100 \mu\text{m}$  which corresponds to the typical thickness of the real films.

This paper stresses the influence of latex stability during the very last stages of drying on surfactant distributions in waterborne polymer films. Within the investigations conducted in this work, both experimentally and theoretically, a coherent view of the phenomena leading to homogeneous or heterogeneous distributions could emerge. However, to what extent these results and interpretations are generalizable to other systems is still unclear.

In order to progress toward a general understanding and predictable results, efforts should be directed in three main directions. First, the resolution, sensitivity, and frequency of experimental methods should increase, especially in the last steps of drying. In many works, including this one, the film still containing water is turbid; it is a “white box” hardly accessible to spectroscopic methods such as Raman or infrared. Crucial pieces of information are lacking, forcing scientists to speculate on major phenomena such as surfactant desorption at the end of drying in the highly concentrated latex. Second, theory should be developed. At this point, limited ranges of polymer volume fractions have been considered (low to 0.64 in Routh’s work, 0.64 to 1 in our work), and particle deformation has not yet been taken into account. More complete, and thus more complex, theories are needed. Third, the simulation tool has not yet been sufficiently used. Simulations would be useful at different scales. At the molecular level, the fate of the surfactant in the highly confined space between close particles could be simulated by molecular dynamics or Monte Carlo methods. At a mesoscopic level, a simulation box in the micrometer range located at various places in the drying film could shed light on the exchange and transport phenomena (particles, surfactant micelles, or molecules) of interest. Only the conjunction of the three approaches, experimental work, theory, and simulation, could lead to significant improvement in this field.

**Acknowledgment.** This work was funded by the EC Framework 6 Integrated Project, NAnostructured waterborne POLymer films with OutstaNding properties (NAPOLEON)

under Contract No. IP 011844-2. We thank Dr. E. Bourgeat Lami and Dr. V. Mellon, University of Lyon, France, for the synthesis of the composite latices (LCPP) and Mr. S. Gree at IS2M, University of Mulhouse, France, for assistance in the Raman analyses.

## References and Notes

- (1) *Fundamentals of Latex Film Formation, Processes and Properties*; Keddie, J. L., Routh, A. F., Eds.; Springer: New York, 2010.
- (2) Aramendia, E.; Barandiaran, M. J.; Grade, J.; Bleasle, T.; Asua, J. M. *Langmuir* **2005**, *21*, 1428–1435.
- (3) Zhao, C.-L.; Holl, Y.; Pith, T.; Lambla, M. *Br. Polym. J.* **1989**, *21*, 155–160.
- (4) Kientz, E.; Holl, Y. *Colloids Surf., A* **1993**, *78*, 255–270.
- (5) Evanson, K. W.; Urban, M. W. *J. Appl. Polym. Sci.* **1991**, *42*, 2287–2296. Evanson, K. W.; Urban, M. W. *J. Appl. Polym. Sci.* **1991**, *42*, 2309–2320. Urban, M. W. *Prog. Org. Coat.* **1997**, *32*, 215–229.
- (6) Zhao, Y.; Urban, M. W. *Macromolecules* **2000**, *33*, 2184–2191. Zhao, Y.; Urban, M. W. *Langmuir* **2000**, *16*, 9439–9447.
- (7) Dreher, W. R.; Zhang, P.; Urban, M. W.; Porzio, R. S.; Zhao, C.-L. *Macromolecules* **2003**, *36*, 1228–1234.
- (8) Rhudy, K. L.; Su, S.; Howell, H. R.; Urban, M. W. *Langmuir* **2008**, *24*, 1808–1813.
- (9) Aramendia, E.; Mallegol, J.; Jeynes, C.; Barandiaran, M. J.; Keddie, J. L.; Asua, J. M. *Langmuir* **2003**, *19*, 3212–3221.
- (10) Tzitzinou, A.; Jenneson, P. M.; Clough, A. S.; Keddie, J. L.; Lu, J. R.; Zhdan, P.; Treacher, K. E.; Satguru, R. *Prog. Org. Coat.* **1999**, *35*, 89–99.
- (11) Lee, W. P.; Gundabala, V. R.; Akpa, B. S.; Johns, M. L.; Jeynes, C.; Routh, A. F. *Langmuir* **2006**, *22*, 5314–5320.
- (12) Gundabala, V. R.; Zimmerman, W. B.; Routh, A. F. *Langmuir* **2004**, *20*, 8721–8727.
- (13) Guignier, D.; Fischer, C.; Holl, Y. *Langmuir* **2001**, *17*, 6419–6425.
- (14) Belaroui, F.; Grohens, Y.; Boyer, H.; Holl, Y. *Polymer* **2000**, *41*, 7641–7645.
- (15) Belaroui, F.; Hirn, M. P.; Grohens, Y.; Marie, P.; Holl, Y. *J. Colloid Interface Sci.* **2003**, *261*, 336–348.
- (16) Xu, G. H.; Dong, J.; Severtson, S. J.; Houtman, C. J.; Gwin, L. E. *J. Phys. Chem. B* **2008**, *112*, 11907–11914.
- (17) Xu, G. H.; Dong, J.; Severtson, S. J.; Houtman, C. J.; Gwin, L. E. *J. Phys. Chem. B* **2009**, *113*, 10189–10195.
- (18) Ludwig, I.; Schabel, W.; Kind, M.; Castaing, J.-C.; Ferlin, P. *AIChE J.* **2007**, *53*, 549–560.
- (19) Arnold, C. Formation of thin polymer films from composite nanocolloids. Ph.D. Thesis, University of Strasbourg, France, 2009.
- (20) Mellon, V. Synthesis and characterization of waterborne polymer/laponite nanocomposite latexes through miniemulsion polymerization. Ph.D. Thesis, University of Lyon, France, 2009.
- (21) Arnold, C.; Ernstrom, M.; Larsson, A.; Marie, P.; Holl, Y., manuscript in preparation.
- (22) Gauer, C.; Wu, H.; Morbidelli, M. *Langmuir* **2009**, *25*, 12073–12083.
- (23) Butt, H. J.; Kuropka, R.; Christensen, B. *Colloid Polym. Sci.* **1994**, *272*, 1218–1223.
- (24) Scalarene, D.; Lazzari, M.; Castelvetro, V.; Chiantore, O. *Chem. Mater.* **2007**, *19*, 6107–6113.
- (25) Patterson, J. M.; Kortylewicz, Z.; Smith, W. T., Jr. *J. Agric. Food Chem.* **1984**, *32*, 782–784.
- (26) Carlsson, G.; Jarnstrom, L.; van Stam, J. *J. Colloid Interface Sci.* **2006**, *298*, 162–171.
- (27) Arnold, C.; Weerakkody, T. G.; Keddie, J. L.; Marie, P.; Holl, Y., manuscript in preparation.
- (28) Doumenc, F.; Guerrier, B. *AIChE J.* **2001**, *47*, 984–993.

JP103347N